Journal of Rock Mechanics and Geotechnical Engineering 15 (2023) 926–936

Contents lists available at ScienceDirect

Journal of Rock Mechanics and Geotechnical Engineering

journal homepage: www.jrmge.cn

Full Length Article

Constitutive modelling of fabric effect on sand liquefaction

Zhiwei Gao [a,*], Dechun Lu [b], Yue Hou [c], Xin Li [a]

[a] James Watt School of Engineering, University of Glasgow, Glasgow, G12 8QQ, UK
[b] Institute of Geotechnical and Underground Engineering, Beijing University of Technology, Beijing, 100124, China
[c] Beijing Key Laboratory of Traffic Engineering, Beijing University of Technology, Beijing, China

ARTICLE INFO

Article history:
Received 16 February 2022
Received in revised form
25 May 2022
Accepted 14 June 2022
Available online 26 June 2022

Keywords:
Sand
Anisotropy
Liquefaction
Finite element modelling
Constitutive model

ABSTRACT

Sand liquefaction under static and dynamic loading can cause failure of embankments, slopes, bridges and other important infrastructure. Sand liquefaction in the seabed can also cause submarine landslides and tsunamis. Fabric anisotropy related to the internal soil structure such as particle orientation, force network and void space is found to have profound influence on sand liquefaction. A constitutive model accounting for the effect of anisotropy on sand liquefaction is proposed. Evolution of fabric anisotropy during loading is considered according to the anisotropic critical state theory for sand. The model has been validated by extensive test results on Toyoura sand with different initial densities and stress states. The effect of sample preparation method on sand liquefaction is qualitatively analysed. The model has been used to investigate the response of a sand ground under earthquake loading. It is shown that sand with horizontal bedding plane has the highest resistance to liquefaction when the sand deposit is anisotropic, which is consistent with the centrifuge test results. The initial degree of fabric anisotropy has a more significant influence on the liquefaction resistance. Sand with more anisotropic fabric that can be caused by previous loading history or compaction methods has lower liquefaction resistance.

1. Introduction

Liquefaction of sand can cause failure of critical infrastructure like earth dams, embankments and bridges. Some submarine landslides have also occurred due to sand liquefaction (Uri et al., 2009). It is well known that the liquefaction resistance of sand is affected by the fabric anisotropy which refers to the particle orientation, contact force networks and void space distribution (e.g. Li and Li, 2009; Gao et al., 2010; Yin et al., 2010; Li and Dafalias, 2012; Gao and Zhao, 2013; Zhao and Guo, 2013; Wei and Wang, 2017). Different inherent anisotropy can be generated by sample preparation methods, compaction or loading history. Experimental evidence has shown that sand with more anisotropic initial fabric has lower liquefaction resistance (Miura and Toki, 1982, 1984; Oda et al., 2001; Yamada et al., 2010; Sze and Yang, 2014; Wei and Wang, 2017; Wang et al., 2021). Recent micromechanical study by Wei and Wang (2017) has shown that more anisotropic sand has a lower coordination number, which makes the soil structure more susceptible to collapse in cyclic loading. For an anisotropic sand sample, the accumulation of strain and excess pore water pressure (EPWP) is dependent on the relative orientation between the bedding plane and principal stress directions (Miura and Toki, 1984; Yoshimine et al., 1998; Wichtmann et al., 2020; Guo et al., 2022). There have also been some centrifuge tests on the effect of anisotropy in sand internal structure on liquefaction in cyclic loading (Yu et al., 2013; Ueda et al., 2019). It is found that the sand ground is more susceptible to liquefaction when the bedding plane is not horizontal.

These experimental studies have highlighted the importance of accounting for anisotropy in assessing the liquefaction of sand ground. To apply this knowledge in practical design, proper modelling of the fabric effect on sand liquefaction is of great importance. Some attempts have been made in this regard. Gao and Zhao (2015) have proposed a constitutive model for sand considering fabric anisotropy and fabric evolution. The model gives a reasonable prediction of loose sand behaviour in cyclic loading but fails to capture the cyclic mobility of dense sand. Wang et al. (2021) have proposed a cyclic sand model based on the anisotropic critical state theory. Liao and Yang (2021) have developed a hypoplastic model that considers the effect of fabric anisotropy. Both models can capture the undrained cyclic response of sand with different

* Corresponding author.
E-mail address: zhiwei.gao@glasgow.ac.uk (Z. Gao).
Peer review under responsibility of Institute of Rock and Soil Mechanics, Chinese Academy of Sciences.

https://doi.org/10.1016/j.jrmge.2022.06.002

densities and initial fabric anisotropy. But all these studies have focused on the soil element response. None of these models has been used in analysing the sand liquefaction in practical boundary value problems. Ueda et al. (2021) have used a multiple mechanism model (Ueda and lai, 2019) to simulate the centrifuge tests reported in Ueda et al. (2019). It is found that the model is not capable of capturing the effect of bedding plane orientation on sand liquefaction. Highly anisotropic permeability has to be considered for capturing the test results. It is assumed that the permeability in the direction perpendicular to the bedding plane is 10 times larger than that in the direction parallel to the bedding plane, which may not be realistic (Chapuis et al., 1989). More research is thus needed to model the fabric effect on sand liquefaction in the field.

This study presents a numerical investigation of the fabric effect on sand liquefaction in earthquakes. The approach in Chaloulos et al. (2019) is used, wherein the constitutive model is proposed and validated by experimental data and then used in real boundary value problems. An anisotropic critical state sand model with fabric evolution is first presented. Sand with more anisotropic fabric is assumed to have lower liquefaction resistance based on the experimental evidence. The model parameters are determined using the test results on Toyoura sand with different densities and initial stress states. The dynamic response of a level sand ground is then simulated, with a focus on the evolution of EPWP at different bedding plane orientations and initial degree of anisotropy.

2. Constitutive model

The constitutive model is based on the bounding surface model proposed by Li (2002). The anisotropic critical state theory (Li and Dafalias, 2012) is employed to account for the effect of fabric anisotropy and fabric evolution. The stress ratio tensor r_{ij} expressed as below is used in the model formulations:

$$r_{ij} = \frac{s_{ij}}{p} = \frac{\sigma_{ij} - p\delta_{ij}}{p} \tag{1}$$

where σ_{ij} is the stress tensor, p is the mean effective stress, s_{ij} is the deviatoric stress tensor, and δ_{ij} is the Kronecker delta ($\delta_{ij} = 1$ for $i = j$ and $\delta_{ij} = 0$ for $i \neq j$). The bounding surface $\bar{f}$ is expressed as (Li, 2002):

$$\bar{f} = \bar{R} / g(\bar{\theta}) - \bar{H} = 0 \tag{2}$$

where $\bar{R} = \sqrt{3\bar{r}_{ij}\bar{r}_{ij}/2}$ with $\bar{r}_{ij}$ being the 'image' stress ratio tensor of the current stress ratio tensor r_{ij}, $\bar{H}$ is the size of the bounding surface, and $g(\bar{\theta})$ is an interpolation function describing the variation of critical state stress ratio with Lode angle $\bar{\theta}$ (Li, 2002):

$$g(\bar{\theta}) = \frac{\sqrt{(1+c^2)^2 + 4c(1-c^2)\sin(3\bar{\theta})} - (1+c^2)}{2(1-c)\sin(3\bar{\theta})} \tag{3}$$

where $c = M_e/M_c$ with M_e and M_c representing the critical state stress ratio in triaxial extension and compression, respectively. The same mapping rule as discussed in Li (2002) is used in the model. The projection centre is the origin of the r_{ij} space at the initial state. It is relocated when unloading occurs. Mroz et al. (1981) were the first to introduce the concept of stress reversal surfaces that corresponds to the relocation of the projection centre in a bounding surface plasticity formulation. This technique was then used by several authors, such as Wang et al. (1990) and Li (2002). The condition of consistency for the cone, $\mathrm{d}\bar{f} = 0$, is expressed as

$$\mathrm{d}\bar{f} = p\bar{n}_{ij}\mathrm{d}\bar{r}_{ij} - \langle L\rangle \bar{K}_p = p\bar{n}_{ij}\mathrm{d}r_{ij} - \langle L\rangle K_p = 0 \tag{4a}$$

where

$$\bar{n}_{ij} = \frac{\frac{\partial\bar{f}}{\partial\bar{r}_{ij}} - \frac{1}{3}\left(\frac{\partial\bar{f}}{\partial\bar{r}_{mn}}\right)\delta_{mn}\delta_{ij}}{\left\|\frac{\partial\bar{f}}{\partial\bar{r}_{ij}} - \frac{1}{3}\left(\frac{\partial\bar{f}}{\partial\bar{r}_{mn}}\right)\delta_{mn}\delta_{ij}\right\|} \tag{4b}$$

where $\bar{n}_{ij}$ is the deviatoric unit tensor defined as the unit norm to $\bar{f}$ at the image stress ratio state $\bar{r}_{ij}$; $\bar{K}_p$ and K_p denote the plastic moduli for the 'image' and current stress state, respectively; L is the loading index; and $\langle\ \rangle$ are the Macauley brackets rendering $\langle L\rangle = L$ for $L > 0$ and $\langle L\rangle = 0$ for $L \leq 0$. The bounding surface size evolves only when r_{ij} is on the bounding surface, and the evolution law is given in Gao and Zhao (2015):

$$\mathrm{d}\bar{H} = \langle L\rangle r_{\bar{H}_1} = \langle L\rangle \left\| \frac{\partial\bar{f}}{\partial\bar{r}_{ij}} - \frac{1}{3}\left(\frac{\partial\bar{f}}{\partial\bar{r}_{mn}}\right)\delta_{mn}\delta_{ij} \right\| \frac{\bar{K}_{p1}}{p} \tag{5}$$

The bounding surface used here has some limitations. When the stress path moves along a stress path parallel to the bounding surface with the projection centre at the origin, there will be no plastic deformation due to the mapping rule. In that case one may want to introduce an additional loading mechanism (e.g. Wang et al., 1990) and the model becomes very complicated.

The plastic strain increment $\mathrm{d}\varepsilon_{ij}^p$ is expressed as

$$\mathrm{d}\varepsilon_{ij}^p = \mathrm{d}e_{ij}^p + \frac{1}{3}\mathrm{d}\varepsilon_v^p\delta_{ij} \tag{6}$$

$$\mathrm{d}e_{ij}^p = \langle L\rangle \bar{n}_{ij} \tag{7}$$

$$\mathrm{d}\varepsilon_v^p = D\sqrt{\frac{2}{3}\mathrm{d}e_{ij}^p\mathrm{d}e_{ij}^p} = \sqrt{\frac{2}{3}}\langle L\rangle D \tag{8}$$

where $\mathrm{d}\varepsilon_v^p$ is the plastic volumetric strain increment, $\mathrm{d}e_{ij}^p$ is the plastic deviatoric strain increment, and D is the dilatancy relationship.

2.1. Fabric anisotropy variable (FAV) and dilatancy state parameter

The model will employ the anisotropic critical state theory (Li and Dafalias, 2012), in which the FAV A and dilatancy state parameter ζ are needed. The FAV A is defined as

$$A = F_{ij}\bar{n}_{ij} \tag{9}$$

$$\zeta = \psi - e_A(A-1) \tag{10}$$

where F_{ij} is the fabric tensor; e_A is a model parameter; $\psi = e - e_c$ is the state parameter defined by Been and Jefferies (1985), in which e_c is the critical state void ratio for the current p and e is the current void ratio. The critical state line in the $e-p$ plane is expressed as (Li and Wang, 1998):

$$e_c = e_\Gamma - \lambda_c\left(\frac{p}{p_a}\right)^\xi \tag{11}$$

where e_Γ, λ_c and ξ are the model parameters; and p_a (= 101 kPa) is the atmospheric pressure. The definition of initial F_{ij} can be found in Li and Dafalias (2012). The fabric tensor is assumed to evolve with plastic deformation as below (Li and Dafalias, 2012):

$$dF_{ij} = \langle L \rangle k_f (n_{ij} - F_{ij}) \tag{12}$$

where k_f is a model parameter that describes the rate of fabric evolution (Li and Dafalias, 2012; Gao et al., 2014). Note that the fabric evolution caused by plastic volumetric strain increment is ignored.

2.2. Plastic modulus and dilatancy relation of the model

The plastic modulus is

$$K_p = \frac{Gh}{\overline{R}} \left[M_c g(\overline{\theta}) \exp(-n\zeta) \frac{\overline{\rho}}{\rho} - \overline{R} \right] \tag{13}$$

where G is the elastic shear modulus; n is a model parameter; and h is a factor for the plastic modulus that is dependent on the void ratio, A and loading history related to the plastic shear strain. Purely elastic sand response is given by the model at the onset of loading direction reversal as K_p is infinite ($\overline{\rho}/\rho \to +\infty$). When $\overline{\rho} = \rho$ (corresponding to the virgin loading or monotonic loading case without stress reversal), $K_p = \overline{K}_p = \frac{Gh}{\overline{R}} [M_c g(\overline{\theta}) e^{-n\zeta} - \overline{R}]$. The term h is

$$h = (1 - h_1 e) \exp(h_2 A) h_c \tag{14}$$

$$h_c = \left(\frac{\rho}{\overline{\rho}} \right)^{20} + \frac{h_3 f(L)}{(1+F)(1+e)} \left[1 - \left(\frac{\rho}{\overline{\rho}} \right)^{20} \right] \tag{15}$$

$$F = \sqrt{F_{ij} F_{ij}} \tag{16}$$

where h_1, h_2 and h_3 are the model parameters; and $f(L)$ is for describing the effect of cyclic loading history on the plastic modulus (Li, 2002). The term $(\rho/\overline{\rho})^{20}$ renders $h_c \approx 1$ for virgin loading and $h_c = h_3 f(L)/[(1+F)(1+e)]$ when the current stress state is within the bounding surface. The expression of $f(L)$ is the same as that in Li (2002):

$$f(L) = \frac{1 - b_3}{\sqrt{(1 - L/b_1)^2 + (L/b_1)/b_2^2}} + b_3 \tag{17}$$

where b_1, b_2 and b_3 are the constants with default values (Li, 2002). It should be emphasized that Eq. (16) is proposed to model cyclic liquefaction of sand, and it does not work for the drained cyclic response. The term $1 + F$ is used to account for the effect of F on the liquefaction resistance of sand in cyclic loading (Gao and Zhao, 2015). It is evident that h decreases as F increases, which means lower stiffness in cyclic loading. This is supported by the experimental evidence (Sze and Yang, 2014; Wei and Wang, 2017; Wang et al., 2021). Different sample preparation methods are found to create sand samples with different initial values of F. Though h_c is assumed to be dependent on F, the model is not able to fully capture the effect of sample preparation on sand behaviour in undrained cyclic loading. To improve the model prediction for the response of sand with different initial values of F, more parameters have to be made fabric-dependent (Papadimitriou et al., 2005; Yang et al., 2008). The term $1 + e$ in Eq. (14) is employed to account for the effect of density on sand response in undrained cyclic loading. It is evident that h_c is smaller when e is higher, indicating lower liquefaction resistance.

The dilatancy relationship is expressed as below, which is based on the original formulation for monotonic loading in Li and Dafalias (2012):

$$D = \frac{d_1}{M_c g(\overline{\theta})} \left[M_c g(\overline{\theta}) \exp(m_d \zeta) \sqrt{\frac{\overline{\rho}}{\rho}} - \overline{R} \right] \tag{18}$$

$$m_d = m \left(\frac{\rho}{\overline{\rho}} \right)^{20} \tag{19}$$

where d_1 and m are the model parameters. The term $m_d = m$ when $\rho/\overline{\rho} = 1$ (virgin loading) and $m_d \approx 0$ when the stress state is within the bounding surface. $m_d \approx 0$ indicates that the phase transformation stress ratio is independent of ζ. This assumption is made based on the observation that the phase transformation stress ratio is almost constant when cyclic mobility occurs (e.g. Oda et al., 2001; Sze and Yang, 2014). Note that though m_d approaches 0 fast as the stress state moves towards the bounding surface, there is no sudden change in D because Eq. (19) is a continuous function. However, when the power used in Eq. (19) is much larger than 20, there will be sudden variation of m_d when $\rho/\overline{\rho}$ is close to 1. The main numerical issue with Eq. (18) is that $\overline{\rho}/\rho$ and D become infinite at the onset of stress reversal (relocation of projection centre). A purely elastic step is thus executed at the stress reversal to avoid such numerical problems.

2.3. Elastic stress strain relations

The elastic shear modulus proposed by Richart et al. (1970) is used in the model:

$$G = G_0 \frac{(2.97 - e)^2}{1 + e} \sqrt{p p_a} \tag{20}$$

where G_0 is a model parameter. The elastic bulk modulus K is a function of G and Poisson's ratio ν:

$$K = G \frac{2(1+\nu)}{3(1-2\nu)} \tag{21}$$

Derivation of the constitutive equations can be found in Li (2002) and will not be given here. The constitutive model has been implemented in Plaxis 2D following the explicit stress integration method (Abbo and Sloan, 1996; Andrianopoulos et al., 2010; Gao et al., 2020). In the implementation, the projection centre update is done following the method in Li (2002). When the projection centre relocation occurs, an elastic step is carried out. The error for stress update in explicit stress integration is set at 10^{-6}. When the mean effective stress approaches a very small value (0.01 kPa), the stress change is assumed 0 when any strain increment is applied to avoid tensile failure in the soil.

3. Model prediction

The model parameters for Toyoura sand under monotonic loading are determined based on the test data in Yoshimine et al. (1998). One group of the test results and model predictions are shown in Fig. 1, where b is the intermediate principal stress variable and α is the major principal stress direction (Yoshimine et al., 1998). The initial degree of anisotropy for Toyoura sand is taken as $F_0 = 0.5$ based on Zhao and Guo (2013). There is only one extra parameter h_3 for cyclic loading, which is determined using the test results shown in Fig. 2 (Kiyota et al., 2008). All the model parameters are given in Table 1. More model predictions for cyclic response of Toyoura sand are shown in Figs. 3–6. The model gives reasonable prediction of the soil behaviour in cyclic loading, though some discrepancy can be found, especially for the stress-strain curves. Better model prediction for cyclic loading can be achieved using a memory surface

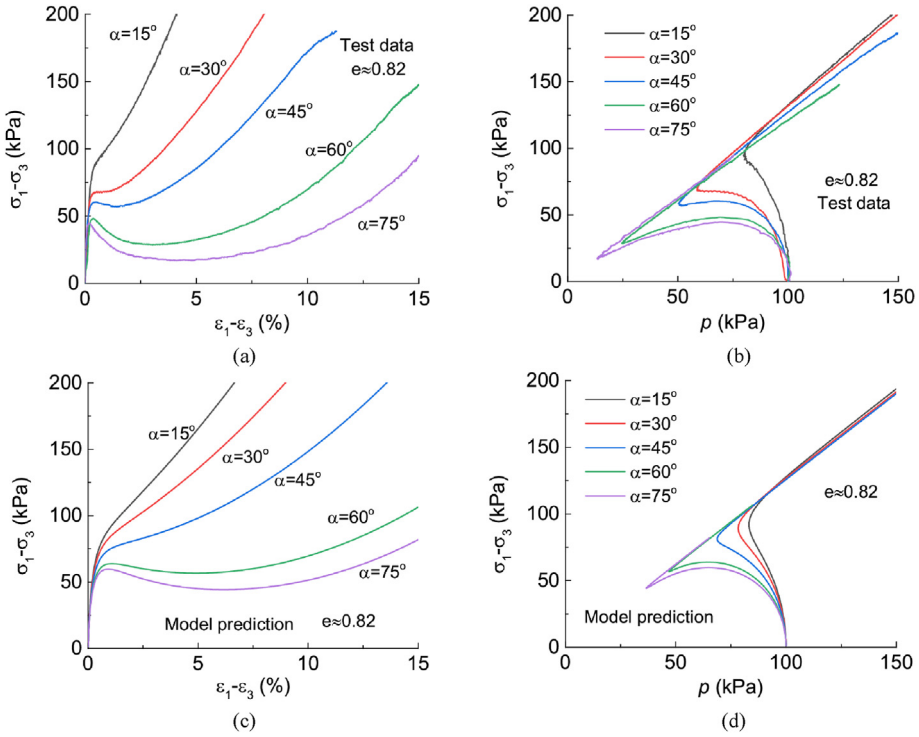

Fig. 1. Model prediction of the undrained sand response in torsional shear with constant b and α (data from Yoshimine et al., 1998): (a, b) Test data, and (c, d) Model prediction.

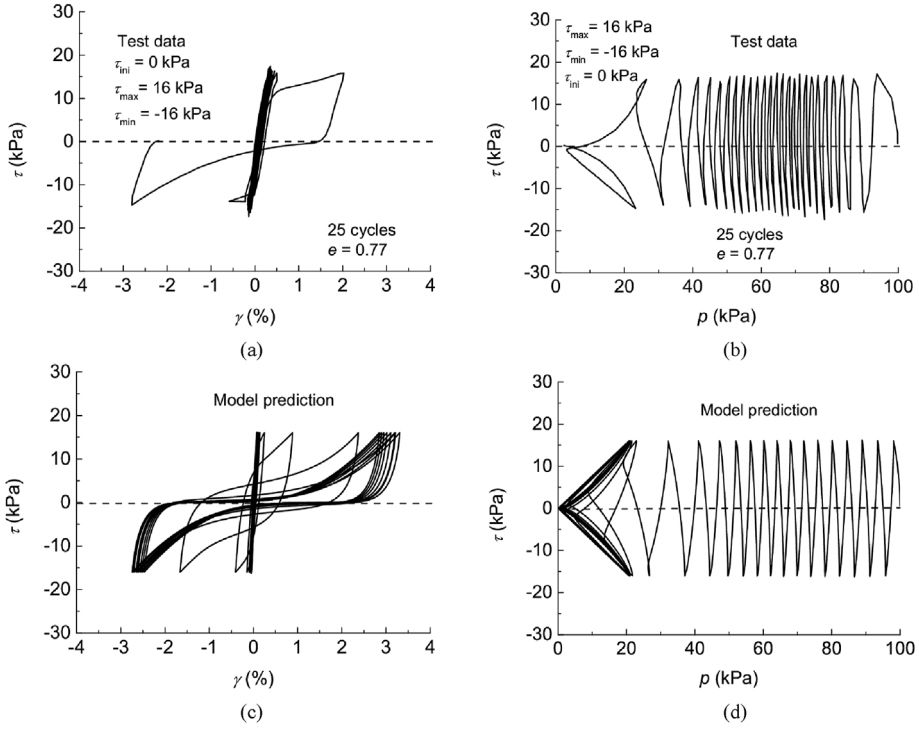

Fig. 2. Model prediction of Toyoura sand in undrained cyclic simple shear with $e = 0.77$ (data from Kiyota et al., 2008): (a, b) Test data, and (c, d) Model prediction.

(Liu et al., 2020; Yang et al., 2020) or improved formulations for the plastic modulus (Wang et al., 1990; Wang and Xie, 2014). But this will inevitably make the model more complex.

Fig. 7 shows the effect of initial degree of anisotropy F_0 on undrained sand response in a cyclic triaxial test. The initial stress state and void ratio of the test are the same as those in Fig. 6. But the soil is assumed to be isotropic at the initial state ($F_0 = 0$). It is shown that different F_0 can be created by changing the sample preparation methods (Miura and Toki, 1984; Sze and Yang, 2014). The initially

Table 1
Model parameters for Toyoura sand.

Critical state	Elasticity	Dilatancy	Hardening	Fabric anisotropy
$M_c = 1.25$	$G_0 = 125$	$d_1 = 0.5$	$h_1 = 0.8$	$e_A = 0.085$
$c = 0.75$	$\nu = 0.1$	$m = 3$	$h_2 = 0.6$	$k_f = 4$
$e_\Gamma = 0.934$			$n = 2$	$F_0 = 0.5$
$\lambda_c = 0.019$			$h_3 = 7$	
$\xi = 0.7$				

isotropic sand shows much higher liquefaction resistance, as there is slower accumulation of excess pore pressure and strain with the number of cycles. This is in agreement with the test data and discrete element simulations (Miura and Toki, 1984; Yamashita and Toki, 1993; Sze and Yang, 2014; Wei and Wang, 2017). It should be mentioned that the current model can only qualitatively describe the effect of sample preparation method on cyclic sand response. Other model parameters may have to be changed to capture the

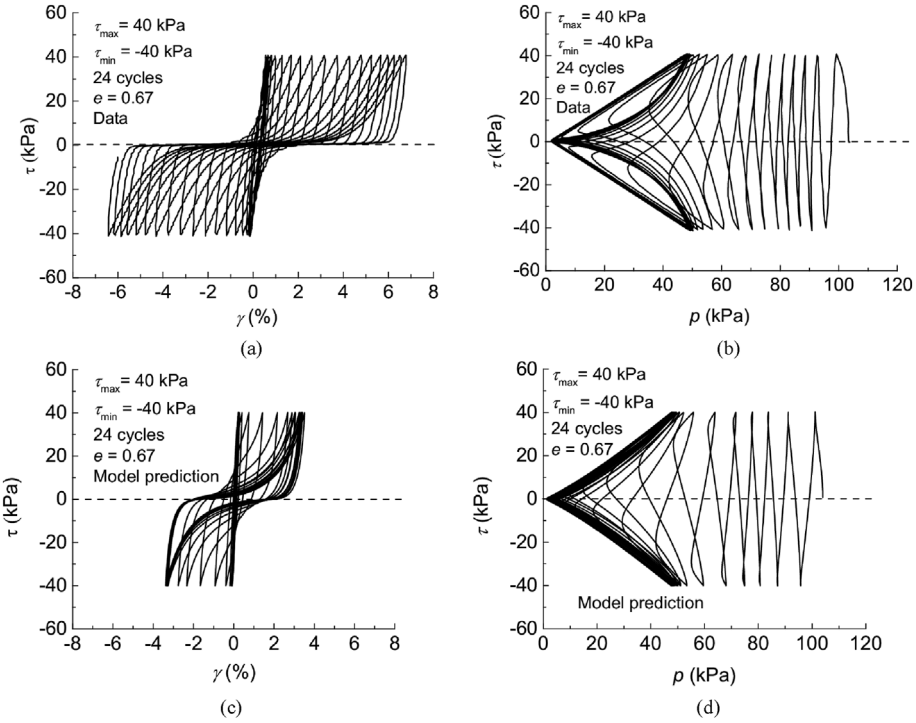

Fig. 3. Model prediction of dense Toyoura sand in undrained cyclic simple shear with $e = 0.67$ (data from Kiyota et al., 2008): (a, b) Test data, and (c, d) Model prediction.

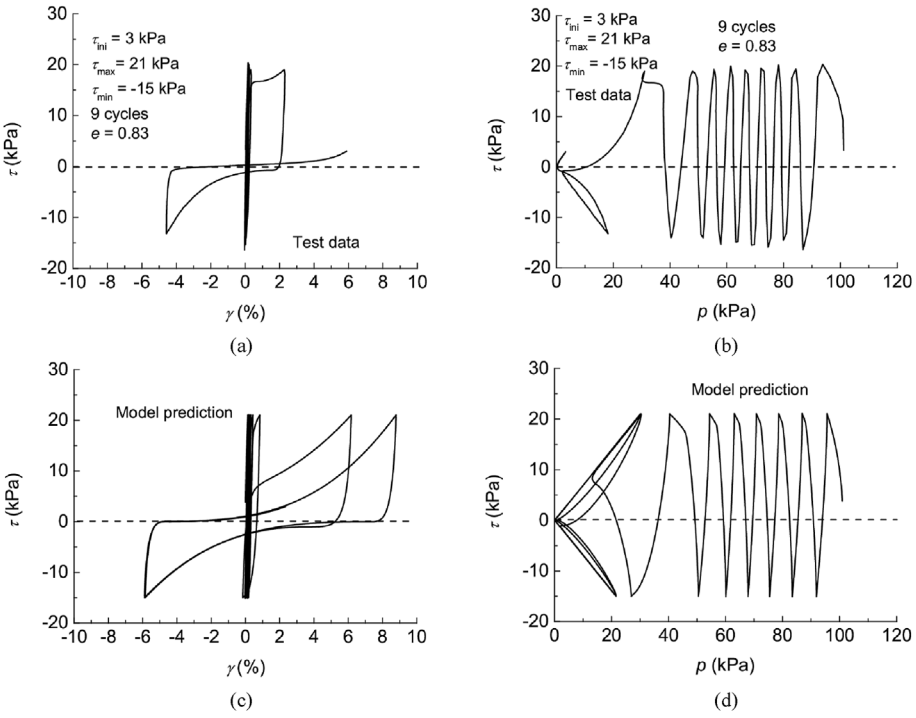

Fig. 4. Model prediction of Toyoura sand in unsymmetric undrained cyclic simple shear with $e = 0.83$ (data from Chiaro et al., 2009): (a, b) Test data, and (c, d) Model prediction.

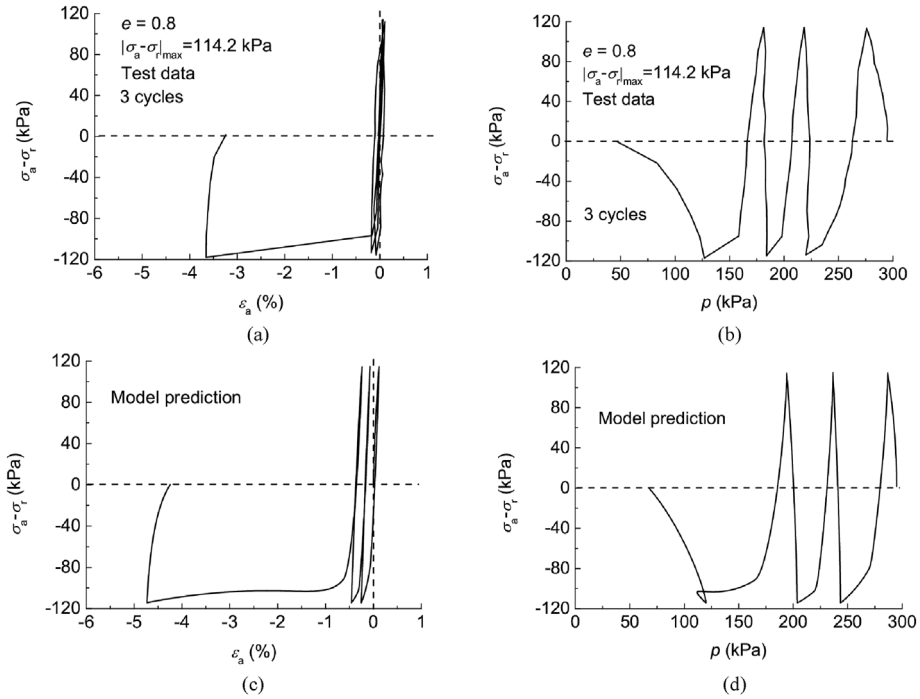

Fig. 5. Model prediction of Toyoura sand in undrained cyclic triaxial compression with $e = 0.8$ (tests by Ishihara et al., 1975 and data extracted from Dafalias and Manzari (2004)); (a, b) Test data, and (c, d) Model prediction.

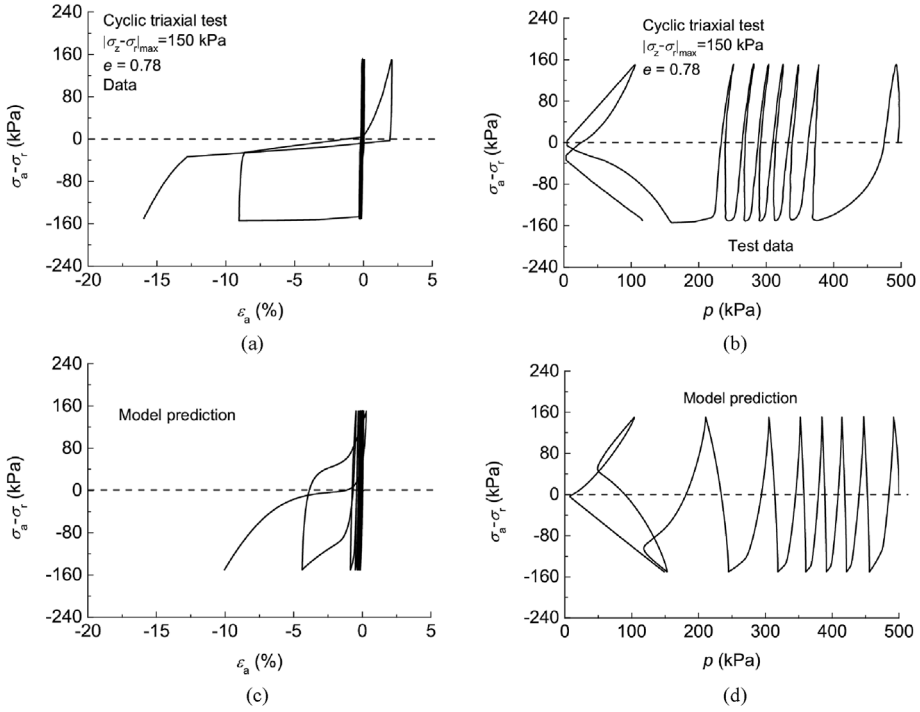

Fig. 6. Model prediction of Toyoura sand in undrained cyclic triaxial compression with $e = 0.78$ (data from Sze and Yang, 2014): (a, b) Test data, and (c, d) Model prediction.

stress-strain relationship of sand prepared by different methods (Papadimitriou et al., 2005; Yang et al., 2008).

Figs. 8 and 9 show the effect of bedding plane orientation on undrained cyclic response of sand in triaxial and simple shear tests. The bedding plane is horizontal when $\beta = 0°$. Fig. 8 indicates that sand is more susceptible to liquefaction when $\beta = 0°$. The direction of strain accumulation is also affected by β, with more negative ε_a at $\beta = 0°$ and more positive ε_a at $\beta = 90°$. This is in agreement with the test data presented in Miura and Toki (1984). Fig. 9 indicates that the liquefaction resistance is lower and there is more shear strain accumulation when $\beta = 45°$. There is no such soil element test data available. But it is shown by recent centrifuge tests that sand ground with horizontal bedding plane is less susceptible to

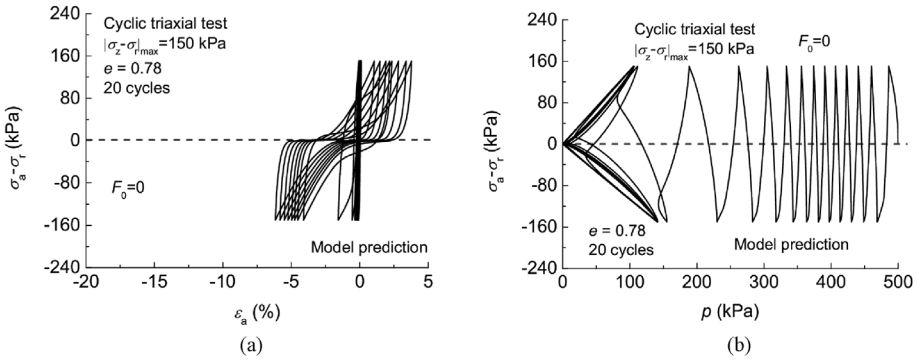

Fig. 7. Effect of initial degree of anisotropy on the behaviour of sand in undrained cyclic triaxial tests ($F_0 = 0$, $e = 0.78$).

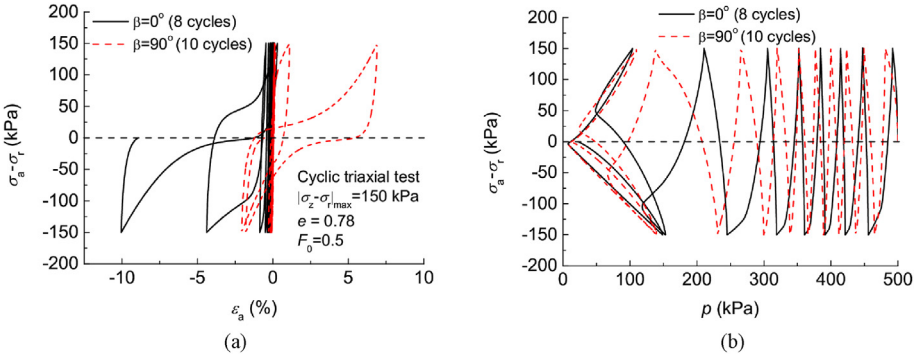

Fig. 8. Effect of bedding plane orientation on the behaviour of sand in undrained cyclic triaxial tests.

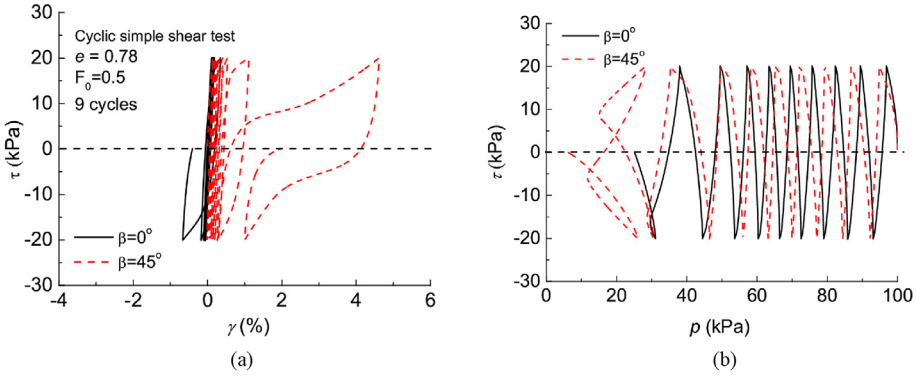

Fig. 9. Effect of bedding plane orientation on the behaviour of sand in undrained cyclic simple shear tests.

liquefaction (Yu et al., 2013; Ueda et al., 2019), which is consistent with the model prediction in Fig. 9. There will be more discussion on this in the following section on finite element modelling of the centrifuge tests.

All the simulations above have focused on the soil response in two-way cyclic loading. In a real boundary value problem, soil elements can be subjected to various loading conditions. One example is the one-way cyclic loading where the shear stress remains either positive or negative. Fig. 10 shows the undrained response of Toyoura sand in one-way cyclic loading. In both triaxial compression and direct simple shear, there is continuous accumulation of the EPWP and degradation of the shear stiffness with loading cycles. This is in agreement with the test results.

4. Dynamic modelling of sand liquefaction

Dynamic liquefaction of sand can occur in different cases, such as on a slope or level ground. The sand liquefaction in a level ground is simulated in the present study. The primary focus of this study is the effect of fabric anisotropy on sand liquefaction, including the bedding plane orientation and initial degree of anisotropy. Plaxis 2D has been used in the modelling.

The sand deposit simulated in this study is 8 m deep and 28 wide (Fig. 11). Some of the soil properties are shown in Table 2. The initial stress state is created by the K_0 method ($K_0 = 0.5$ is assumed). The total soil unit weight is $\gamma_{sat} = 19.3$ kN/m^3 and the ground water level is at the ground surface. The sand permeability $k = 0.0004$ m/s is obtained from Ueda et al. (2019). The initial void ratio e_0 and initial fabric are assumed uniform in the soil. Since the

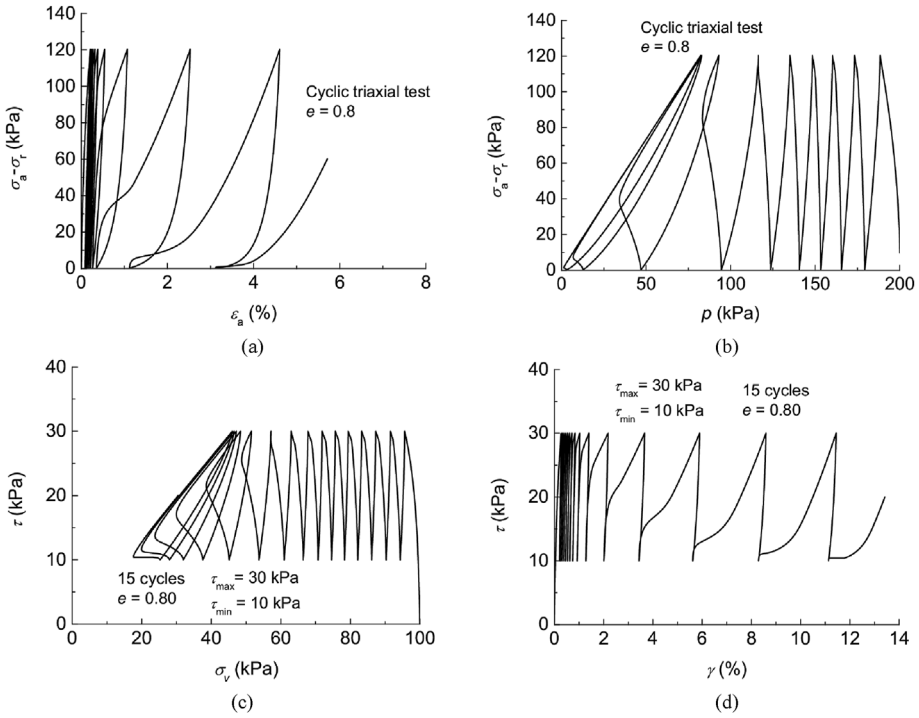

Fig. 10. Model prediction of undrained sand response in one-way cyclic loading: (a, b) Triaxial compression tests, and (c, d) Direct simple shear tests.

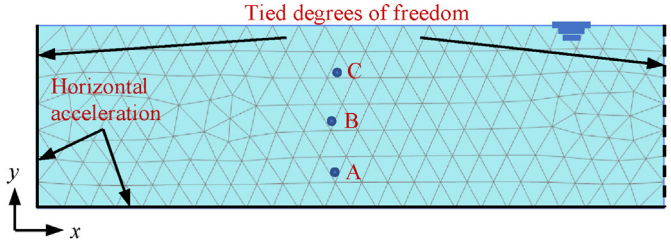

Fig. 11. Mesh size and boundary conditions for the dynamic modelling.

Table 2
Soil properties for the dynamic simulations.

Property	Value
Permeability	$k = 0.0004$ m/s
Initial earth pressure coefficient	$K_0 = 0.5$
Initial void ratio	$e_0 = 0.73$ ($D_r = 66\%$)
Saturated unit weight	$\gamma_{sat} = 19.3$ kN/m^3

soil is cross-anisotropic, the initial fabric tensor can be defined as below when the bedding plane is horizontal:

$$F_{ij} = \begin{bmatrix} F_{xx} & F_{xy} & F_{xz} \\ F_{yx} & F_{yy} & F_{yz} \\ F_{zx} & F_{zy} & F_{zz} \end{bmatrix} = \sqrt{\frac{2}{3}} \begin{bmatrix} -F_0/2 & 0 & 0 \\ 0 & F_0 & 0 \\ 0 & 0 & -F_0/2 \end{bmatrix} \quad (22)$$

where z represents the direction perpendicular to the x-y plane. When the bedding plane orientation changes, the components of F_{ij} need to be obtained using orthogonal transformation. $F_0 = 0.5$ has been used in the predictions above, wherein the initial stress state is isotropic. In the dynamic simulations, initially anisotropic stress state is used and $F_0 = 0.6$ is assumed because the soil fabric is more anisotropic after K_0 consolidation (Gao et al., 2020, 2021).

Six-node triangle elements with pore water pressure are used. The small strain formulation is used in the modelling. The mesh size is approximately 1 m. There are two phases in the modelling. In the first phase, the initial stress state is created, and all the state variables are set. The initial stress state is assumed to be on the bounding surface. Standard boundary conditions are applied in this phase, with the bottom fixed and two vertical sides free to move vertically. In the second phase, dynamic analysis with consolidation is performed. During this phase, the vertical displacement is fixed while horizontal acceleration is applied at the bottom (Fig. 11). The acceleration history is obtained through personal communication with Dr. Katerina Ziotopoulou at the University of California Davis (Fig. 12). Note that the acceleration history has been modified using baseline correction to minimize the overall drift of the displacement. The same horizontal acceleration is applied at the two vertical sides to simulate the rigid boundary condition reported in the centrifuge tests (Yu et al., 2013; Ueda et al., 2019). Water drainage is only allowed at the top boundary.

Fig. 13 shows the evolution of EPWP at different locations (see Fig. 11). It is evident that the EPWP accumulates faster when the bedding plane is not horizontal. There is a small difference in EPWP accumulation at $\beta = 45°$ and 90°, which is consistent with the

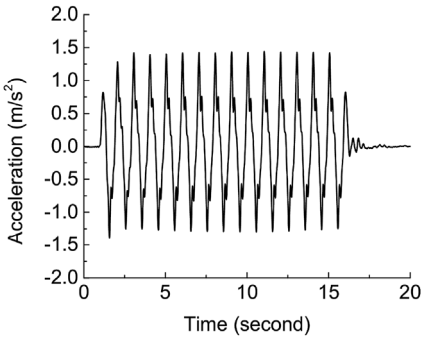

Fig. 12. Horizontal acceleration history.

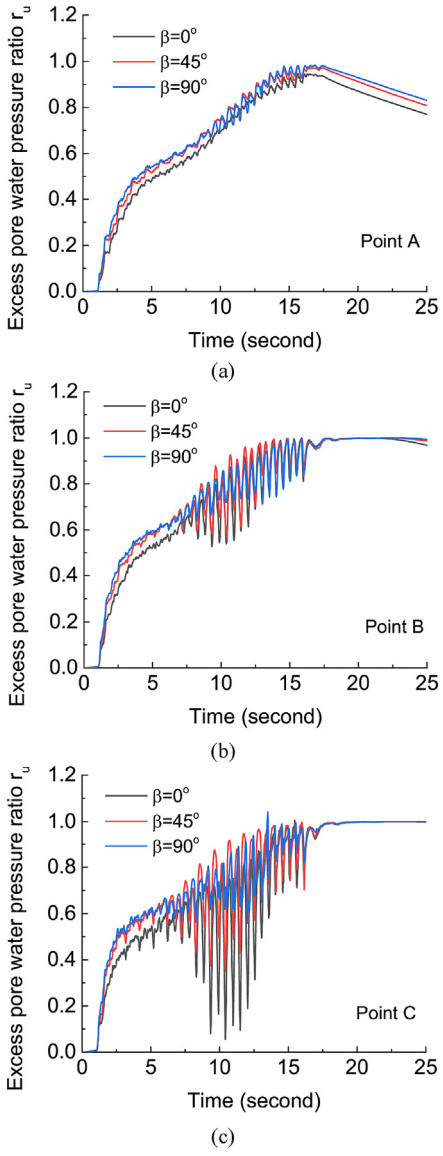

Fig. 13. Effect of bedding plane orientation on EPWP evolution at different locations: (a) Point A, (b) Point B, and (c) Point C.

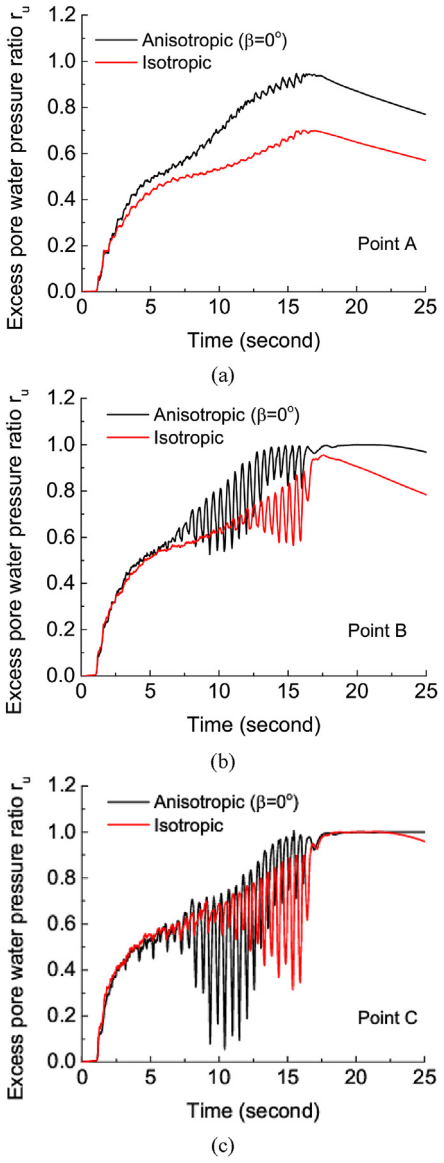

Fig. 14. Effect of initial degree of anisotropy F_0 on EPWP evolution: (a) Point A, (b) Point B, and (c) Point C.

centrifuge test results (Yu et al., 2013; Ueda et al., 2019). But the centrifuge tests have shown more significant influence of bedding plane orientation on EPWP evolution in general. There are several reasons for this discrepancy: (a) Sand elements in the dynamic modelling are subjected to a loading condition similar to cyclic direct simple shear. The EPWP evolution in cyclic simple shear predicted by the model is insensitive to the bedding plane orientation before phase transformation occurs (Fig. 9b). This makes the evolution of EPWP similar for different bedding plane orientations. The model formulations can be further improved if there were soil element test data for the simulations shown in Fig. 9b. The permeability anisotropy has effect on EPWP evolution. Ueda et al. (2021) have shown that consideration of anisotropic permeability can better capture the effect of bedding plane orientation on EPWP development. But there is a lack of data regarding the permeability anisotropy with different bedding plane orientations. The degree of permeability anisotropy assumed in Ueda et al. (2021) appears to be too high. (b) The distribution of initial void ratio and fabric anisotropy, which has a dramatic influence on EPWP evolution, can be different as the bedding plane orientation changes due to the sample preparation methods.

Fig. 14 shows the effect of initial fabric anisotropy on sand liquefaction in the dynamic modelling. The same soil properties in Table 2 have been used in the simulations. The initially isotropic sand has $F_0 = 0$. When the soil is initially isotropic, it shows much higher liquefaction resistance. The difference is more obvious in deeper soil layers. This agrees with the soil element tests reported in the literature. This indicates that a proper sample preparation method has to be used in centrifuge tests to reproduce the soil response in the field. Even though the void ratio is the same, sand samples prepared by different methods (corresponding to different F_0) can have very different liquefaction resistance.

5. Conclusions

A bounding surface constitutive model for describing the effect of fabric anisotropy on sand liquefaction is proposed. The evolution of fabric anisotropy with plastic shear strain is considered based on

the anisotropic critical state theory for sand. The model gives higher liquefaction resistance when the initial soil fabric is more isotropic, while other conditions are the same. The model has been validated by the undrained test results of Toyoura sand in both monotonic and cyclic loading with different densities and confining pressures. The model can qualitatively capture the effect of sample preparation method on liquefaction of sand.

The model has been used to investigate the response of a sand ground in dynamic modelling. When the sand ground is anisotropic, the soil shows higher liquefaction resistance when the bedding plane is horizontal, which is consistent with the centrifuge test observations. The effect of bedding plane orientation on sand liquefaction predicted by the model is less significant than that observed in centrifuge tests. Better model prediction can be obtained by considering the anisotropy in permeability. The initial degree of fabric anisotropy is found to have a significant influence on the liquefaction resistance. An isotropic sand ground is much less susceptible to liquefaction under earthquake loading when other conditions are the same. Therefore, a proper sample preparation method must be used in element or centrifuge tests for reproducing the sand liquefaction behaviour in the field.

The model tends to give good prediction for the effective stress paths but not the stress and strain relationship. More work needs to be done to improve the model performance in this regard. A possible option is to use the memory surface concept (Liu et al., 2020; Yang et al., 2020). Determination of the model parameters is also a challenge. One can use the optimization method developed in the literature for more efficient parameter determination (Jin et al., 2016, 2018; Yin et al., 2017, 2018).

Declaration of competing interest

The authors declare that they have no known competing financial interests or personal relationships that could have appeared to influence the work reported in this paper.

Acknowledgments

The authors would like to acknowledge Dr. Katerina Ziotopoulou at the University of California Davis and Dr. Kyohei Ueda at Kyoto University for providing their centrifuge test data. The 2nd author would like to acknowledge the support of the National Natural Science Foundation of China (Grant No. 52025084).

References

Abbo, A.J., Sloan, S.W., 1996. An automatic load stepping algorithm with error control. Int. J. Numer. Methods Eng. 39 (10), 1737–1759.
Andrianopoulos, K.I., Papadimitriou, A.G., Bouckovalas, G.D., 2010. Explicit integration of bounding surface model for the analysis of earthquake soil liquefaction. Int. J. Numer. Anal. Methods GeoMech. 34 (15), 1586–1614.
Been, K., Jefferies, M.G., 1985. A state parameter for sands. Geotechnique 35 (2), 99–112.
Chaloulos, Y.K., Papadimitriou, A.G., Dafalias, Y.F., 2019. Fabric effects on strip footing loading of anisotropic sand. J. Geotech. Geoen. Eng. 145 (10), 04019068.
Chapuis, R.P., Gill, D.E., Baass, K., 1989. Laboratory permeability tests on sand: influence of the compaction method on anisotropy. Can. Geotech. J. 26 (4), 614–622.
Chiaro, G., Kiyota, T., De Silva, L.I.N., Sato, T., Koseki, J., 2009. Extremely large post-liquefaction deformations of saturated sand under cyclic torsional shear loading. In: Earthquake Geotechnical Engineering Satellite Conference. Alexandria, Egypt.
Dafalias, Y.F., Manzari, M.T., 2004. Simple plasticity sand model accounting for fabric change effects. J. Eng. Mech. 130 (6), 622–634.
Gao, Z.W., Zhao, J.D., 2013. Strain localization and fabric evolution in sand. Int. J. Solid Struct. 50 (22–23), 3634–3648.
Gao, Z.W., Zhao, J.D., Yao, Y.P., 2010. A generalized anisotropic failure criterion for geomaterials. Int. J. Solid Struct. 47 (22–23), 3166–3185.
Gao, Z.W., Zhao, J.D., Li, X.S., Dafalias, Y.F., 2014. A critical state sand plasticity model accounting for fabric evolution. Int. J. Numer. Anal. Methods GeoMech. 38 (4), 370–390.
Gao, Z.W., Lu, D.C., Du, X.l., 2020. Bearing capacity and failure mechanism of strip footings on anisotropic sand. J. Eng. Mech. 146 (8), 04020081.
Gao, Z.W., Zhao, J.D., Li, X., 2021. The deformation and failure of strip footings on anisotropic cohesionless sloping grounds. Int. J. Numer. Anal. Methods GeoMech. 45 (10), 1526–1545.
Gao, Z.W., Zhao, J.D., 2015. Constitutive modeling of anisotropic sand behavior in monotonic and cyclic loading. J. Eng. Mech. 141 (8), 04015017.
Guo, N., Yang, F., Yang, Z.X., Zhao, S., 2022. Deformation characteristics of inherently anisotropic granular media under repeated traffic loading: a DEM study. Acta Geotech. 2022 17, 3377–3395.
Ishihara, K., Tatsuoka, F., Yasuda, S., 1975. Undrained deformation and liquefaction of sand under cyclic stresses. Soils Found. 15 (1), 29–44.
Jin, Y.F., Yin, Z.Y., Wu, Z.X., Zhou, W.H., 2018. Identifying parameters of easily crushable sand and application to offshore pile driving. Ocean Eng. 154, 416–429.
Jin, Y.F., Yin, Z.Y., Shen, S.L., Hicher, P.Y., 2016. Selection of sand models and identification of parameters using an enhanced genetic algorithm. Int. J. Numer. Anal. Methods GeoMech. 40 (8), 1219–1240.
Kiyota, T., Sato, T., Koseki, J., Abadimarand, M., 2008. Behavior of liquefied sands under extremely large strain levels in cyclic torsional shear tests. Soils Found. 48 (5), 727–739.
Li, X.S., 2002. A sand model with state-dependent dilatancy. Geotechnique 52 (3), 173–186.
Li, X.S., Dafalias, Y.F., 2012. Anisotropic critical state theory: the role of fabric. J. Eng. Mech. 138 (3), 263–275.
Li, X.S., Li, X., 2009. Micro–macro quantification of the internal structure of granular materials. J. Eng. Mech. 135 (7), 641–656.
Li, X.S., Wang, Y., 1998. Linear representation of steady-state line for sand. J. Geotech. Geoenviron. Eng. 124 (12), 1215–1217.
Liao, D., Yang, Z.X., 2021. Hypoplastic modeling of anisotropic sand behavior accounting for fabric evolution under monotonic and cyclic loading. Acta Geotech 16 (7), 2003–2029.
Liu, H., Diambra, A., Abell, J.A., Pisanò, F., 2020. Memory-enhanced plasticity modeling of sand behavior under undrained cyclic loading. J. Geotech. Geoenviron. Eng. 146 (11), 04020122.
Miura, S., Toki, S., 1982. A sample preparation method and its effect on static and cyclic deformation- strength properties of sand. Soils Found. 22 (1), 61–77.
Miura, S., Toki, S., 1984. Anisotropy in mechanical properties and its simulation of sands sampled from natural deposits. Soils Found. 24 (3), 69–84.
Mroz, Z., Norris, V.A., Zienkiewicz, O.C., 1981. An anisotropic, critical state model for soils subject to cyclic loading. Geotechnique 31 (4), 451–469.
Oda, M., Kawamoto, K., Suzuki, K., Fujimori, H., Sato, M., 2001. Microstructural interpretation on reliquefaction of saturated granular soils under cyclic loading. J. Geotech. Geoenviron. Eng. 127 (5), 416–423.
Papadimitriou, A.G., Dafalias, Y.F., Yoshimine, M., 2005. Plasticity modeling of the effect of sample preparation method on sand response. Soils Found. 45 (2), 109–123.
Richart, F.E., Hall, J.R., Woods, R.D., 1970. Vibrations of Soils and Foundations. Prentice-Hall, Englewood Cliffs, NJ, USA.
Sze, H., Yang, J., 2014. Failure modes of sand in undrained cyclic loading: impact of sample preparation. J. Geotech. Geoenviron. Eng. 140 (1), 152–169.
Ueda, K., Hyodo, J., Sato, K., Sugiura, Y., 2021. Seismic response analysis of liquefiable sandy ground considering inherent anisotropy's influence. In: International Conference of the International Association for Computer Methods and Advances in Geomechanics. Springer, Cham.
Ueda, K., Iai, S., 2019. Constitutive modeling of inherent anisotropy in a strain space multiple mechanism model for granular materials. Int. J. Numer. Anal. Methods GeoMech. 43 (3), 708–737.
Ueda, K., Uratani, K., Iai, S., 2019. Influence of inherent anisotropy on the seismic behavior of liquefiable sandy level ground. Soils Found. 59 (2), 458–473.
Uri, S., Lee, H.J., Geist, E.L., Twichell, D., 2009. Assessment of tsunami hazard to the US East Coast using relationships between submarine landslides and earthquakes. Mar. Geol. 264 (1–2), 65–73.
Wang, G., Xie, Y., 2014. Modified bounding surface hypoplasticity model for sands under cyclic loading. J. Eng. Mech. 140 (1), 91–101.
Wang, R., Cao, W., Xue, L., Zhang, J., 2021. An anisotropic plasticity model incorporating fabric evolution for monotonic and cyclic behavior of sand. Acta Geotechnica 16, 43–65.
Wang, Z.L., Dafalias, Y.F., Shen, C.K., 1990. Bounding surface hypoplasticity model for sand. J. Eng. Mech. 116 (5), 983–1001.
Wei, J.T., Wang, G., 2017. Discrete-element method analysis of initial fabric effects on pre-and post-liquefaction behavior of sands. Géotech. Lett. 7 (2), 161–166.
Wichtmann, T., Steller, K., Triantafyllidis, T., 2020. On the influence of the sample preparation method on strain accumulation in sand under high-cyclic loading. Soil Dynam. Earthq. Eng. 131, 106028.
Yamada, S., Takamori, T., Sato, K., 2010. Effects on reliquefaction resistance produced by changes in anisotropy during liquefaction. Soils Found. 50 (1), 9–25.
Yamashita, S., Toki, S., 1993. Effects of fabric anisotropy of sand on cyclic undrained triaxial and torsional strengths. Soils Found. 33 (3), 92–104.
Yang, M., Taiebat, M., Dafalias, Y.F., 2020. SANISAND-MSf: a sand plasticity model with memory surface and semifluidised state. Geotechnique 72 (3), 1–20.

Yang, Z.X., Li, X.S., Yang, J., 2008. Quantifying and modelling fabric anisotropy of granular soils. Geotechnique 58 (4), 237–248.
Yin, Z.Y., Chang, C.S., Hicher, P.Y., 2010. Micromechanical modeling for effect of inherent anisotropy on cyclic behavior of sand. Int. J. Solid Struct. 47 (14–15), 1933–1951.
Yin, Z.Y., Jin, Y.F., Shen, S.L., Hicher, P.Y., 2018. Optimization techniques for identifying soil parameters in geotechnical engineering: comparative study and enhancement. Int. J. Numer. Anal. Methods GeoMech. 42 (1), 70–94.
Yin, Z.Y., Jin, Y.F., Shen, S.L., Huang, H.W., 2017. An efficient optimization method for identifying parameters of soft structured clay by an enhanced genetic algorithm and elastic-viscoplastic model. Acta Geotech 12 (4), 849–867.
Yoshimine, M., Ishihara, K., Vargas, W., 1998. Effects of principal stress direction and intermediate principal stress on undrained shear behavior of sand. Soils Found. 38 (3), 179–188.
Yu, H., Zeng, X., Li, B., Ming, H., 2013. Effect of fabric anisotropy on liquefaction of sand. J. Geotech. Geoenviron. Eng. 139 (5), 765–774.
Zhao, J.D., Guo, N., 2013. Unique critical state characteristics in granular media considering fabric anisotropy. Geotechnique 63 (8), 695–704.

Dr. Zhiwei Gao is a Senior Lecturer at the James Watt School of Engineering at University of Glasgow, UK. He obtained his BEng and MSc (Research) degrees from the Beihang University in China, and his PhD degree in Civil Engineering from the Hong Kong University of Science and Technology. His research has been focusing on computational geomechanics. Specifically, he has been working on constitutive modelling of sand accounting for the effect of anisotropy and evolution. The constitutive model has been used for finite element modelling of practical boundary value problems. He has worked with the industry to develop a design for lightweight rock catch fences through laboratory tests, finite element modelling and full-scale field tests. Based on the outcome of this project, a remote monitoring system was developed. He is currently working on geotechnical problems associated with climate change and offshore wind power: (i) mechanics of gassy clay and the associated geotechnical problems (submarine landslides); and (ii) finite element modelling of offshore foundation response subjected to long-term cyclic loading.